Nucleic Acids Research, Vol. 19, No. 25 7145–7154

Parallel-stranded DNA under topological stress: rearrangement of $(dA)_{15}\cdot(dT)_{15}$ to a $d(A\cdot A\cdot T)_n$ triplex

Jan Klysik+, Karsten Rippe and Thomas M.Jovin*
Department of Molecular Biology, Max Planck Institute for Biophysical Chemistry, Postfach 2841, W-3400 Göttingen, FRG

ABSTRACT

DNA oligonucleotides with appropriate sequences can form a stable duplex in which the two strands are paired in a parallel orientation instead of as the conventional antiparallel double helix of B-DNA. In parallel-stranded DNA (ps-DNA) base pairing is noncanonical with the glycosidic bonds in a *trans* orientation. The two grooves are equivalent. We have synthesized DNA duplexes consisting of a central parallel-stranded $(dA)_{15}\cdot(dT)_{15}$ tract flanked by normal antiparallel regions, and ligated them into the pUC18 plasmid. The effect of negative supercoiling on the covalently closed circular molecules was studied by two-dimensional agarose gel electrophoresis and by chemical modification with OsO_4-pyridine (Os,py) and diethylpyrocarbonate (DEPC). The following results were obtained: (i) The ps insert, and by inference ps-DNA in general, adopts a right handed helical form. (ii) Upon increasing the negative superhelix density ($-\sigma$) to > 0.03 the 15 bp ps insert undergoes a major transition leading to a relaxation corresponding to a reduction in twist of ~ 2.5 helical turns. The transition free energy is ~10 kcal/mol. (iii) The chemical modification pattern of the resulting structure suggests that the purine strand folds back and associates with the pyrimidine strand, forming a novel intramolecular triplex structure consisting of d(A·A·T) base triplets. A model for the triplex conformation is proposed and its thermodynamic properties are analyzed by statistical mechanics.

INTRODUCTION

The parallel orientation of certain duplex-forming DNA sequences is well established [reviewed in (1, 2)]. The conformation denoted here as parallel-stranded DNA (ps-DNA) was predicted theoretically by Pattabiraman (3) and first examined experimentally with a series of hairpin molecules in which 3′-p-3′ and 5′-p-5′ phosphodiester bonds were introduced in order to enforce a parallel orientation of the $d(A)_{10}\cdot d(T)_{10}$ stem (4). These studies were extended to linear two-stranded duplexes (5–7) some of which also had interspersed d(G·C) base pairs (8). The base pairing in ps-DNA is of the *trans*-Crick-Watson type (*t-CW*, synonymous with *reverse* Watson-Crick), as confirmed by Raman spectroscopy (9), ^{1}H-NMR (10) and chemical methylation (4). The thermodynamic stability of ps-DNA is only slightly lower than that of the aps reference molecules (4–7), facilitating numerous studies of the spectroscopy [reviewed in (1)], drug binding (1,5,10), substrate properties (11), chemical reactivities (12), and other features of this novel structure. However, there have been no reports as yet of parallel-stranded duplexes embedded in conventional antiparallel stranded (aps) DNA sequences nor of the effect of topological stress on the ps conformation. In order to pursue this question we synthesized and characterized oligonucleotides that could form a duplex with a central $d(A)_{15}\cdot d(T)_{15}$ tract in a parallel orientation. The aps flanking sequences were complementary to certain restriction sites in the polylinker region of the pUC18 vector. These constructs were ligated into covalently closed circles and subjected to topological stress by negative supercoiling. The properties of such molecules are presented here.

MATERIALS AND METHODS

Oligonucleotide synthesis and characterisation

The oligonucleotides were synthesized and purified as described previously (7). The purity of the isolated [^{32}P] end-labeled oligonucleotides was established by electrophoresis under denaturing conditions (7). More than 95% was the full length product. The 3′-p-3′ and a 5′-p-5′ bonds of fragment P5 (Fig. 1) were introduced by using the 5′-β-cyanoethyl-3′-dimetoxytrityl thymidine phosphoramidite during synthesis of the central 15 dTs whereas all the other additions were made with the the normal 5′-dimethoxytrityl-3′-β-cyanoethyl protected phosphoramidites. Synthesis of the 5′-β-cyanoethyl-3′-dimetoxytrityl thymidine phosphoramidite was essentially as described in (4), but with the exception that the 5′-OH group of thymidine was protected with *tert.*-butyl-diphenylchlorsilane instead of *tert.*-butyl-dimethyl-chlorsilane. For a detailed description of synthesis see (13).

Polyacrylamide gel electrophoresis of oligonucleotides under native conditions was carried out in 14% polyacrylamide (5% crosslinking), 90 mM Tris-borate, pH 8.0, 2 mM $MgCl_2$

* To whom correspondence should be addressed

+ Present address: Texas A & M University, Institute of Biosciences and Technology, 2121 Holcombe, Houston, TX 77030, USA

(TBM) and at 20°C. The digitized images of the fluorescent bands were obtained by exciting the gel with an ultraviolet transilluminator and recording the emission with a Series 200 slow-scan digital CCD camera (Photometrics, Tucson, AZ) and appropriate bandpass filters.

Preparation of plasmids with the parallel-stranded insert

All enzymes were from New England Biolabs unless otherwise noted. The units of enzyme activity are defined according to the manufacturers specifications. For the preparation of the covalently closed circular plasmid with the 15 base pair parallel-stranded dA·dT insert two different protocols, designated as scheme I and scheme II (Fig. 3) were used. In scheme I (Fig. 3A, left panel) the pUC18 plasmid was digested to completion with *Eco*O 109 and then with *Bsp*M I. We found that reversing the order of digestion results in incomplete digestion of the vector probably due to slow *Bsp*M I kinetics of the supercoiled plasmid. The longer vector fragment was isolated by gel electrophoresis on a 5% polyacrylamide gel (5% crosslinking) and recovered either by extraction or by electroelution. It was then ligated with a 10 fold molar excess of ps-P3·P5 duplex in 50 mM NaCl, 10 mM $MgCl_2$, 50 mM Tris-HCl, pH 7.6, 1 mM ATP (buffer A) and 400 units ml^{-1} of DNA ligase. Completion of the reaction was monitored by digestion of the products with *Ssp* I and *Pvu* II. The synthetic fragments do not have 5'-phosphates; therefore only one strand can be ligated to each side of the vector. The ligation products were subjected to FPLC (Pharmacia) chromatography using a HR 5/5 MonoQ column in order to separate the excess of unligated synthetic fragments from the vector. The gradient was 0−0.3 M NaCl (10 min) followed by 0.3−0.8 M NaCl (80 min) in 20 mM Tris·HCl, pH 7.6, 0.1 mM EDTA at a flow rate of 0.25 ml min^{-1}. The synthetic fragment was end labeled using [^{32}P]γ-ATP and T4 polynucleotide kinase in buffer A with ATP replaced by [^{32}P] γ-ATP). Unlabeled ATP was added to a concentration of 1 mM after 15 min. The solution was then diluted 20 times with H_2O to 1 μg ml^{-1} DNA and heated to 70°C for 10 min. At this temperature the unligated strand of the synthetic duplexes dissociates but the plasmid does not denature. After cooling to room temperature 1/10 of the volume of 10×buffer B (50 mM Tris-HCl, pH 7.6, 1 mM ATP, 20 mM DTT) was added. The circularization reaction was performed with 400 units ml^{-1} of DNA ligase overnight at 16°C. The products were precipitated with 3 volumes of ethanol and dissolved in 10 mM Tris-HCl buffer, pH 7.6.

In the second procedure designated as scheme II (Fig. 3A, right panel), pUC18 was digested with *Pst* I. The linearized plasmid was then ligated with a 10 fold molar excess of the ps-P5·P6 duplex in buffer A and 400 units ml^{-1} of DNA ligase. The synthetic duplex fragment was preformed from kinased P5 (indicated by a dot in Fig. 3A) and unkinased P6. Completion of the ligation was monitored by restriction digestion analysis with *Pvu* II. The ligation was stopped by phenol extraction followed by ether extraction (3 times) and ethanol precipitation. The DNA was then digested with *Xma* I and subjected to chromatography at 45°C on a Waters 600E HPLC system with a Gen-Pak Fax column. The gradient was 0−0.5 M NaCl (10 min) followed by 0.5−1.0 M NaCl (20 min) at a flow rate of 0.75 ml min^{-1}; both solutions also contained 20 mM Tris·HCl, pH 7.6, 0.1 mM EDTA. This step separated the desired molecule carrying the synthetic duplex at one end from an excess of the synthetic fragment, the dimer of the synthetic fragment, and the shorter *Xma* I digestion product. The material obtained was kinased (in buffer A using an excess of T4 polynucleotide kinase), diluted with buffer B to a DNA concentration of 1 μg ml^{-1} and ligated overnight at 16°C (400 units ml^{-1} of DNA ligase). Ligation products were concentrated 10 fold by n-butanol extraction and precipitated with 3 volumes of ethanol. The material was used for CsCl/EtBr banding. Supercoiled DNA was collected, dialysed, and additionally purified by ion exchange HPLC chromatography. The recovered material was precipitated with 3 volumes of ethanol and dissolved in 10 mM Tris-HCl Buffer, pH 7.6. About 10% of the initial pUC18 DNA material was found in the finally purified closed circles. The sequences of the inserts in pPS-PX1 and pPS-PP1 as well as the corresponding regions in pAPS-EB1 and pAPS-PX1 were confirmed by the standard Maxam and Gilbert (14) method.

Two-dimensional gel electrophoresis

The agarose gels were run in 1.5% agarose in TBE buffer at room temperature as described before (15) and supplemented with 0.2 μg ml^{-1} chloroquine in the second dimension. Topoisomers differing in superhelicity and therefore in the extent of a structural transition are resolved in the first dimension. In the second orthogonal direction, a significant degree of unwinding is effected by an intercalating agent, thereby reversing local transitions and their associated perturbations of electrophoretic mobility. The topoisomer samples were generated from mixtures of radiolabeled ps plasmids and unlabeled aps plasmids by incubation with calf thymus toposiomerase I (BRL) at different ethidium bromide concentrations according to Ref. (16). The ethidium and topoisomerase were removed by phenol extraction followed by ether extraction.

The important experimental variable in the 2-D gel analysis of topoisomers is the linking number *difference* ΔLk (< 0 for negatively supercoiled closed circular DNA) defined here in terms of a normalized quantity, the superhelix density $\sigma = \Delta Lk/Lk_0 = (Lk - Lk_0)/Lk_0 = (\Delta Tw + Wr)/Lk_0$ [reviewed in (17)]. ΔTw is the change in twist and Wr the writhe induced by deviations from Lk_0, the linking number of an idealized relaxed ($Wr = 0$) DNA of N base pairs; $Lk_0 = N/h_0$. The helical repeat h_0 is 10.5 base pairs/turn for B-DNA under standard ionic and temperature conditions (18). The value of σ is derived from the difference between each topoisomer number and the computed apex (corresponding to Lk_0) of the distribution (Fig. 4). A decrease in twist ($\delta\Delta Tw < 0$) induced by a conformational transition in a covalently closed molecule is compensated by a release of negative supercoils and a reduction in the magnitude of writhe ($\delta Wr > 0$), according to the conservation condition $\delta\Delta Tw + \delta Wr = 0$. The writhe component is the principle determinant of electrophoretic mobility differences between topoisomers in agarose gels resolved by the 2-D method (19). The mean change in ΔTw ($\delta\Delta Tw$, denoted $<\Delta Tw>$ to correspond with general usage in the literature) is given by the apparent $\delta\Delta Lk$ between a given topoisomer undergoing a transition and the value calculated at the position with the same electrophoretic mobility (and thus Wr) in the distribution of unrelaxed topoisomers. The apparent change in superhelix density $\Delta\sigma$ (Eq. 2) equals $-<\Delta Tw>h_0/N$.

Chemical modifications

The plasmids (0.5 μg) in the relaxed (re) or in the supercoiled (sc) state was suspended in 10 μl of 20 mM Tris-HCl buffer and treated either with 1.1 μl of OsO_4-pyridine reagent (20 mM

OsO_4, 20% pyridine) for 15 min at room temperature or with 1.1 μl of DEPC for 30 min at room temperature. The samples were extracted with ether, precipitated with 4 volumes of ethanol, washed with 75% ethanol, and digested with *Hind* III and *Sst* I (BRL) or *Eco*R I and *Sph* I depending on the strand to be analyzed. After labelling with [^{32}P] α-dATP and Klenow fragment the products were separated on a 5% polyacrylamide gel and the shorter digestion products were extracted, treated with piperidine and loaded on a sequencing gel after dissolving in the formamide. The same number of counts was loaded on each channel. The supercoiled plasmid had a mean σ of about −0.06 as calculated from the topoisomeric ladder of the aps control plasmid pAPS-PX1. The autoradiographs were digitized with a CCD camera system and the images were processed as described previously (12). These data are shown in panels C and D of Fig. 5.

RESULTS

Synthesis and characterization of aps-ps-aps DNA duplexes

The synthetic duplexes used in this study are shown in Fig. 1. The strand P5 contains a 3′-p-3′ and a 5′-p-5′ phosphodiester linkage that invert the orientation of the 15 dT intervening residues. Upon hybridizing P5 with strands P3 or P6, duplex molecules are formed that contain a parallel-stranded $(dA)_{15}\cdot(dT)_{15}$ insert [ps-P3·P5, ps-P5·P6; the designation ps refers only to the central $(dA)_{15}\cdot(dT)_{15}$ tract]. Antiparallel reference duplexes of the same length and sequence (aps-P3·P4, aps-P4·P6) were obtained by replacing P5 with strand P4.

In order to confirm that the $(dA)_{15}\cdot(dT)_{15}$ segment adopts a ps conformation, we examined the fluorescence elicited upon binding the intercalator ethidium bromide and the groove-binder bisbenzimidazole BBI-258 (Hoechst 33258) to duplexes resolved on a native polyacrylamide gel (Fig. 2A). In addition, we determined the temperature dependent ultraviolet absorption spectra (Fig. 2B, 2C). Ethidium bromide binds very well to ps-DNA; the opposite holds for BBI-258 (1,2,4−6,10). It is apparent from the ethidium bromide stained gel (Fig. 2A, Et designated lanes) that the combinations with the ps insert ps-P3·P5 and ps-P5·P6 as well as the aps-P3·P4 and aps-P4·P6 reference molecules migrate as duplexes in the native gel. No fluorescence is perceived upon staining ps-P3·P5 and ps-P5·P6 with BBI-258, but the aps references show the normal enhancement of fluorescence upon drug binding. These results are in accordance

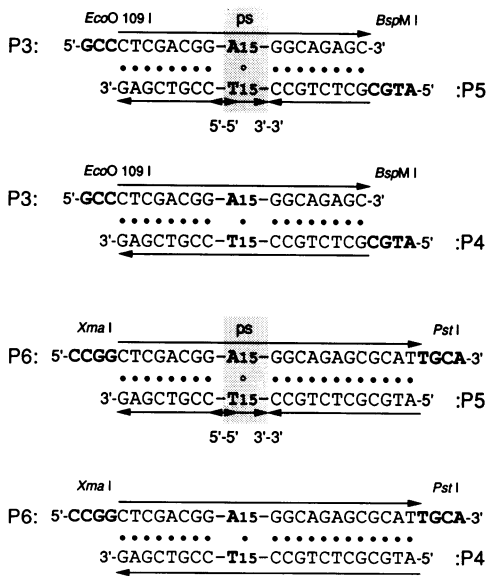

Fig. 1. Sequences of synthetic oligonucleotides and their duplexes. The *cis*-Watson-Crick (*c-CW*) base-pairs of the antiparallel duplexes are denoted by the symbol ● and the *trans*-Crick-Watson base-pairs (*t-CW*) of the parallel-stranded duplexes by the symbol ○. The fragment P5 contains a 3′-p-3′ and 5′-p-5′ linkages that leads to a reversal of the polarity of the central 15 dT residues.

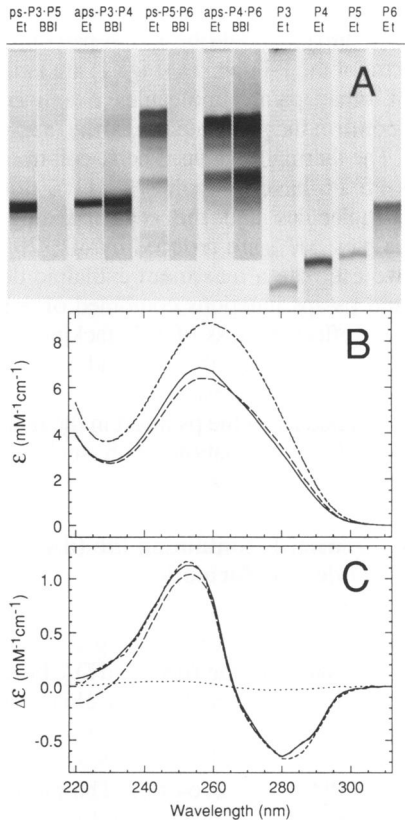

Fig. 2. Characterization of synthetic duplexes. **(A)** Native gel electrophoresis and drug binding of oligonucleotides and their duplexes. The amount of DNA applied to each lane was 0.2 nmole strands. The gel was first stained with 0.15 μg ml^{-1} Hoechst 33258 (BBI-258) in TBM (lanes denoted with BBI). The lanes with the single strands showed no fluorescence. After destaining the gel was restained in 1 μg ml^{-1} ethidium bromide in TBM (lanes denoted with Et). Note that the ps-P5·P6 and the aps-P4·P6 duplex can form dimers via the *Xma* I site with 4 dG·dC base pairs overhang, accounting for the upper electrophoretic bands. **(B)** Ultraviolet absorption spectra. Native spectra at 10°C of ps-P5·P6 (—) and aps-P4·P6 (− − −) and denatured spectra at 80°C of ps-P5·P6 (- - -) and of aps-P4·P6 (· · · ·). Ultraviolet absorption measurements were made in 50 mM NaCl, 0.1 mM EDTA and 10 mM Na-cacodylate, pH 7.0, as described previously (7). The T_m determined under these conditions was 57°C for ps-P5·P6, 66°C for aps-P4·P5, 50°C for ps-P3·P5 and 61°C for aps-P3·P4 at a total strand concentration of 0.6 μM. The molar extinction coefficients of the oligonucleotides were calculated according to Ref. (8): P3, P6 (8.3); P4, P6 (8.5); the units are mM base^{-1} cm^{-1} at 264 nm in the denatured state (70°C in 10 mM Na-cacodylate, pH 7.0, + 0.1 M NaCl). The corresponding value for the denatured duplexes at 80°C is 8.5 mM base^{-1} cm^{-1}. **(C)** Difference spectra of [ps-P5·P6 − aps-P4·P6]·31/15 at 10°C (—) and at 80°C (· · · ·) and of [ps-P3·P5 − aps-P3·P4]·35/15 at 10°C (− − −). The multiplication by 31/15 and 35/15, respectively, compensates for the expected fraction of the duplex in the ps conformation. The difference spectrum of a 25-nt linear ps duplex and its aps reference in 0.1 M NaCl at 10°C (- - -) is shown as a reference for the canonical ps-aps difference spectrum [data adapted from Ref. (7)].

with other data (1,2,4−6,10) showing that the drug binds readily to the (dA)·(dT) sequences only in an aps orientation. BBI-258 has a strong preference for dA·dT rich DNA, and thus is also excluded from the the aps flanking regions of ps-P3·P5 and ps-P5·P6 in which dG·dC base pairs predominate.

The ultraviolet absorption spectra of ps-P3·P5 and ps-P5·P6 at 10°C in 50 mM NaCl solutions exhibit the characteristic blue shift of ps-DNA (1,2,4−7) upon comparison with the references aps-P3·P4 and aps-P4·P6 (Fig. 2B, 2C). The spectra of the two denatured molecules are virtually identical. The difference spectrum (ps − aps) in the native state has a positive peak at 250−255 nm, an isosbestic point at 265−270 nm, and a negative peak at 280−285 nm (Fig. 2C). Taking into account that only about half of the duplex should be in the ps conformation, the difference spectra of the P-duplexes (Fig. 1) are indistinguishable from those of other ps/aps molecules examined previously (Fig. 2C) and confirm the postulated tripartite (aps-ps-aps) block conformation. The thermally induced helix-coil transitions of ps-P3·P5 and ps-P5·P6 have midpoints 9−11°C lower than the aps reference molecules and the corresponding van't Hoff transition enthalpies ΔH_{vH} are reduced by 10−20%. From the limited data, we estimate a maximum enthalpic destabilization at the aps-ps and ps-aps junctions combined of ~9 kcal/mole. This value could reflect the loss of 1/2 stacking interaction per junction, for example, along the pyrimidine strand with the 5′-p-5′ and 3′-p-3′ phosphodiester bonds. The hyperreactivity of the terminal dT residues of the ps insert in the relaxed plasmids (see below) would be compatible with such an effect and indicative of its restricted, local nature.

Construction of plasmids containing the $(dA)_{15}\cdot(dT)_{15}$ tract in a parallel-stranded conformation

A diagram of all plasmids is presented in Fig. 3B. Two of these, pAPS-EB1 (total length N = 2305 bp) and pAPS-PX1 (N = 2702 bp), contain inserts that have the $(dA)_{15}\cdot(dT)_{15}$ block in normal, antiparallel orientation and were made by cloning the synthetic duplexes aps-P3·P4 and aps-P4·P6, respectively. Both served as reference molecules for studying the behavior of pPS-EB1, pPS-PX1 and pPS-PP1 (N = 2764 bp). The plasmids with the ps inserts could not be obtained by cloning, since it is not possible to propagate 3′-p-3′ and 5′-p-5′ linkages in *E. coli* cells. Thus, we developed an *in vitro* procedure to obtain enough material according to schemes I and II outlined in Fig. 3A. The first protocol produced pPS-EB1 plasmids in analytical amounts, sufficient for labelling and 2-D agarose gel electrophoresis. The second procedure, which we found to be more reproducible, was devised to obtain pPS-PX1 in the quantities required for chemical modification and sequencing. Both strategies resulted in circular plasmids that incorporate the ps $(dA)_{15}\cdot(dT)_{15}$ insert but placed in a somewhat different sequence environment of the pUC18 vector. A third construct, pPS-PP1 (Fig. 3B) has two inverted repeats of the ps-P5·P6 duplex located in the *Pst* I restriction site of the pUC18 vector.

Two-dimensional gel electrophoresis analysis

We analyzed the ps constructs by the standard method of two-dimensional agarose gel electrophoresis in which a ladder of positively and negatively supercoiled topoisomers is resolved. At negative superhelix densities above a given threshold, local conformational transitions are potentiated leading to a reduction in the global underwinding of the the DNA helix [reviewed in (20−23)]. The accompanying decrease in supercoiling is

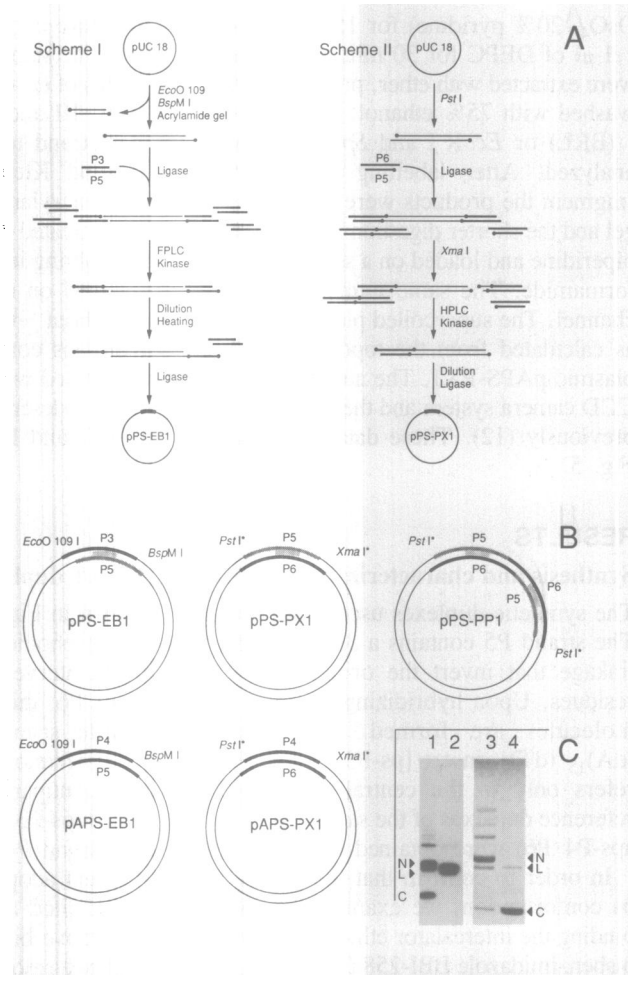

Fig. 3. (**A**) Preparation scheme for the covalently closed circular plasmid with the 15 base pairs parallel-stranded dA·dT insert. The phosphate at the 5′-end is indicated by a dot. *Scheme I*: The pUC18 plasmid was cut with *Eco*O 109 and then with *Bsp*M I. The longer vector fragment was isolated on a polyacrylamide gel and ligated with a 10 fold molar excess of ps-P3·P5 duplex. The synthetic fragments do not have 5′-phosphates. Therefore, only one strand can be ligated to each side of the vector. The excess of unligated synthetic fragments was separated from the vector by ion exchange chromatography. After the kinase reaction and dilution the unligated strand of the synthetic duplex was separated by heating to 70°C and the circularization reaction was performed after cooling. *Scheme II*: pUC18 was completely digested with *Pst* I. The linearized plasmid was ligated with a 10 fold molar excess of the ps-P5·P6 duplex in which only P5 was kinased. The DNA was then digested with *Xma* I and subjected to ion chromatography to separate the desired molecule carrying the synthetic duplex from shorter sequences. The material obtained was kinased and ligated overnight and purified, ligated and further processed as described unter Material and Methods. (**B**) Plasmids used in this study. pPS refers to the plasmids containing the ps $(dA)_{15}\cdot(dT)_{15}$ insert whereas pAPS indicates that the plasmid carries the aps reference insert. The additional letters (*i.e.*, EB, PX and PP) refer to the restriction sites of the vector used to incorporate the synthetic sequences (*Eco*O 109-*Bsp*M I, *Pst* I-*Xma* I and *Pst* I-*Pst* I, respectively). Note that the *Pst* I and *Xma* I restriction sites are not regenerated in the plasmid with the insert as indicated by the star (*). The plasmids pAPS-EB1 and pAPS-PX1 were obtained by cloning. pPS-EB1 was constructed according to scheme I whereas pPS-PX was made according to Scheme II. Preparation of pPS-PP1 was according to scheme II but the *Xma* I digestion step was omitted. Maxam and Gilbert sequencing revealed the presence of the expected sequence of inserts of constructs. (**C**) Agarose gel analysis of pPS-EB1 and pPS-PX1. The inset shows a picture of the material obtained according to scheme I (lanes 1, 2 autoradiograph) or scheme II (lanes 3, 4 ethidium bromide staining) analyzed on a 1% agarose gel in 40 mM Tris-acetate, 1 mM EDTA, pH 8.0 (TAE) and 4 μg ml^{-1} of ethidium bromide. The letters refer to the following species C: covalently closed circles, N: nicked circles; L: linear species. Lane 1: nondigested pPS-EB1 preparation. Lane 2: same as 1 but linearized with *Pvu* II. Lane 3: DNA recovered from the upper band (linear DNA) of the CsCl gradient of the pPS-PX1 preparation. Lane 4: DNA recovered from the bottom band (supercoiled DNA) of the CsCl gradient of the pPS-PX1 preparation.

evidenced by dramatic and abrupt decreases in electrophoretic mobility. These effects have been observed and quantitated in the case of the B−Z transition (19,24,25), hairpin extrusion of inverted repeat or self-complementary sequences (cruciformation) (26,27), and disproportionation of palindromic oligopurine·oligopyrimidine sequences into triple-stranded H-DNA (28−31)

The 2-D gel analysis of plasmids containing the $(dA)_{15}\cdot(dT)_{15}$ tract in the ps and in the aps conformations is shown in Fig. 4. Topoisomers +3 to ~ −14 of the pPS-EB1 and the pAPS-EB1 plasmids (outlined) are presented in panel A. The electrophoretic mobilities coincide up to topoisomer −5, from which we conclude that the ps $(dA)_{15}\cdot(dT)_{15}$ insert consists of a right-handed double helix. In order to estimate the helical repeat $h_{o,ps}$ of the ps insert one can decompose the inverse mean value $\langle h_o\rangle^{-1}$ for the relaxed state of the plasmid pPS-EB1 (Fig. 4A) in terms of the weighted average of the two aps (vector) and ps (insert) helical segments and a total excess twist b_{ps} accounting for possible distortions at the two aps-ps and ps-aps junctions. We define b_{ps} as a deviation from the standard helical twist, $1/h_{o,aps}$, and ascribe it the units of aps helical turns. Thus,

$$\langle h_o\rangle^{-1} = [(N-15)/h_{o,aps} + 15/h_{o,ps} + b_{ps}]/N. \quad (1)$$

where N is the total length of the plasmid. Assuming that $|b_{ps}| \leq 0.5$, that the analytical resolution is better than 0.1 helical turn, and that the superposed topoisomers have the same integer linking numbers, we estimate that $|h_{o,ps} - h_{o,aps}| \leq 4$. That is, the relative difference in the helical repeat is ≤40%. Force field calculations have provided estimates of h_o for a parallel-stranded duplex and its antiparallel reference molecule of ~ 9 (4,8). The accepted literature value for B-DNA is 10.5 (18).

More direct evidence for the right-handed nature of the ps insert is provided by the transition observed at the higher negative superhelix densities. It starts with topoisomer −6 in Fig. 4A and is characterized by the appearance of a species that migrates more slowly in the first electrophoretic dimension. By topoisomer −8, the transition within the synthetic insert is virtually complete; the reduced migration of the single spot corresponds to a decrease of > 2 in the apparent linking number difference.

The quantitative relationships calculated in terms of the superhelix density σ and helical twist change $\langle\Delta Tw\rangle$ are shown in Fig. 4C. Data are also included from experiments with the plasmids pPS-PX1 and pAPS-PX1 (panel B; the transition occurs at a somewhat higher topoisomer number because the DNA is 17% longer) and the constructs with two inserts pPS-PP1 and pAPS-PP1. The characteristics of the transition are as follows. (i) The single-insert ps plasmids show a major transition with a midpoint at $\sigma_{tr} \approx -0.036$ (points about curves *a1*, *a2*). The maximal unwinding corresponds to ~2.5 turns, *i.e.*, a $\Delta\sigma \approx +0.01$. The transition free energy can be estimated from the known quadratic dependence of the free energy of supercoiling.

$$\Delta G_{tr} = \lim_{-\sigma\to\infty}\{-\delta\Delta G_s = -NK'[(\sigma + \Delta\sigma)^2 - \sigma^2] = -NK'\Delta\sigma(2\sigma + \Delta\sigma)\} \quad (2)$$

where $K' = 1150h_{o,aps}^{-2}$ $RT = 10RT$ for $N > 2000$ (18); R is the gas constant and T the absolute temperature. We obtain $\Delta G_{tr} = 10 \pm 1$ kcal/mol. (ii) The transition occurs at neutral pH in moderate (< 0.1 M) concentrations of NaCl or low (2 mM) concentrations of $MgCl_2$ (data not shown). (iii) In experiments with the pPS-EB1 plasmid (Fig. 4A), 20−40% of topoisomers −7 to −9 migrates with a progressively reduced mobility defining a second apparent transition with a lower midpoint $\sigma_{tr} \approx -0.030$ but the same final degree of unwinding (points not shown in Fig. 4C). In the case of the pPS-PX1 plasmid, but not pPS-EB1, some smearing instead of a distinctive splitting of topoisomers −7 to −9 is observed (Fig. 4B). Whether this process involves an alternative, possibly metastable structure or a progressive σ-dependent deformation of the aps-ps-aps insert is as yet unclear. (iv) The double-insert ps plasmid pPS-PP1 also shows a major transition (points about curve *b*) occurring at a

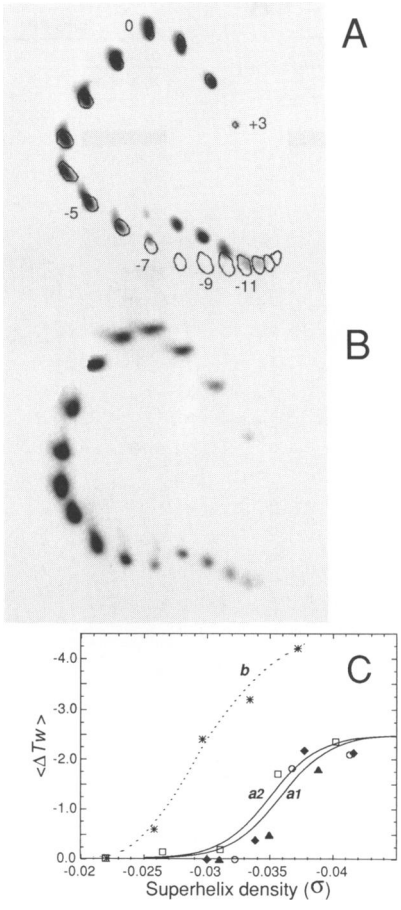

Fig. 4. Two-dimensional (2-D) agarose gel electrophoresis. (**A**) pPS-EB1 and pAPS-EB1 (non-radioactive, outlined), (**B**) pPS-PX1. (**C**) Plot of unwinding $\langle\Delta Tw\rangle$ versus superhelix density σ. pPS-EB1 (different experiments: □,○); pPS-PX1 (different experiments: ♦,▲); pPS-PP1 (*). Panels **A** and **B** are images of optical densities acquired and processed digitally (12); in some cases spot positions were determined visually from photographic enlargements. Data were from autoradiographs (ps plasmids) and from photographs of ethidium stained gels (aps plasmids). The first dimension is from top to bottom, and the second from left to right. The positions of the centers of mass for each spot *i* (the slowest was designated topoisomerase number $tn_{i,\,slowest} = 0$) were fit by a power series function so as to obtain by interpolation the apparent non-integer value tn_o of the apex in the first dimension. The linking number difference ΔLk_i of the *i*th topoisomer is then given by $tn_i - tn_o$. The apparent relaxation of a given topoisomer was assessed by comparison with the superposed aps distribution, when available, or by extrapolation to the apparent ΔLk of a non relaxed species with the same electrophoretic mobility. The solid lines in **C** represent fits by variable iteration to the experimental data using the statistical mechanical formulation of Eqs. 3−6. Curves *a1* and *a2* correspond to $N = 2305$ (pPS-EB1) and 2702 (pPS-PX1), respectively. Fixed parameters (valid for 25°C, 0.09−0.1 M NaCl) were: $n = 15$; $s_{ps} = 2.5$ [calculated from Refs. (1,2,4−7)]; $s_{aps} = 5$ (52); $\sigma_d = 1.5\times10^{-7}$ [$= \sigma_c K_{el}^{le}$ of Refs. (51,52); calculated for 0.1 M NaCl]; $l_{min} = 3$ (53). Adjustable variables were: $b_o = -1.1$ (curves *a1*, *a2*) or −1.2 (curve *b*); $\sigma_j\sigma_t$ and s_t are discussed in text. Curve *b* represents the transition in the plasmid pPS-PP1 ($N = 2764$) that carries two ps $(dA)_{15}\cdot(dT)_{15}$ inserts and was drawn freehand.

lower negative superhelix density ($\sigma_{tr} \approx -0.030$) compared to pPS-EB1 and pPS-PX1. The extent of unwinding $-\langle \Delta Tw \rangle$ is > 4, implying that both ps inserts are involved.

Modification with OsO_4-pyridine (Os,py) and diethyl pyrocarbonate (DEPC)

We examined the structural basis for the transitions of the ps inserts in a series of chemical modification experiments using base-specific probes applied extensively in studies of supercoiled molecules [reviewed in (15,32)]. Two of the best-characterized of these are the osmium tetroxide-pyridine (Os,py) complex (33) and diethyl pyrocarbonate (34,35). Os,py reacts mainly with dT residues forming osmate ester derivatives and is a very effective agent for detecting B–Z junctions (15,33), cruciform loops (15,36) and the looped out regions associated with intramolecular triplex H-DNA (30,37–40). DEPC carbetoxylates N7 of dA residues (and dG, to a lesser extent) (15,34,35) and detects Z-segments within circular plasmids (34,35), cruciform loops (41), and single-stranded regions of H-DNA forming sequences (30,37–40). Os,py and DEPC modified bases can be detected with single nucleotide resolution by cleaving the DNA backbone with hot piperidine (32–35). We limited our studies to these two particular chemicals since the ps insert was composed exclusively of dA and dT residues.

Modification experiments performed on the pPS-PX1 and the pPS-PP1 plasmids are depicted in Fig. 5. In the relaxed state, the pyrimidine tract shows a weak and uniform Os,py modification pattern of dT residues within the $d(A)_{15} \cdot d(T)_{15}$ parallel segment, with increased reactivity of thymines at the 3′-p-3′ and 5′-p-5′ phosphodiester linkages (panel A, lane 5; panel B, lanes 1,5; panel C). The latter effect is probably due to local deformational (junctional) effects upon the helical structure in this region, as discussed in relation to the

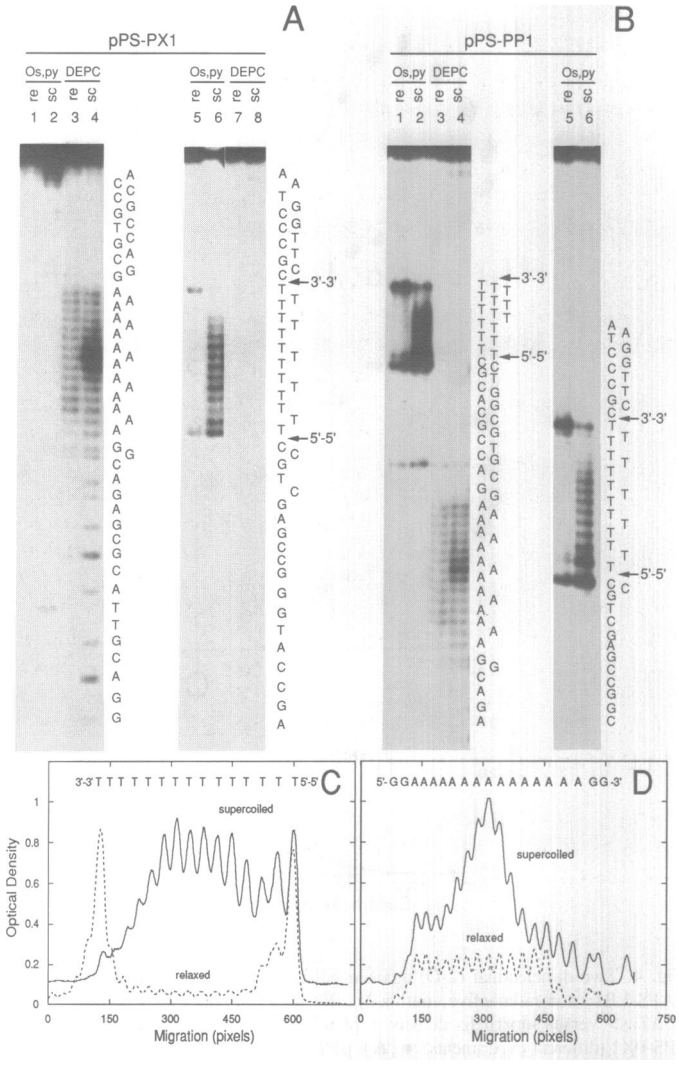

Fig. 5. Chemical modification of plasmids pPS-PX1 and pPS-PP1. **(A)** pPS-PX1 in the relaxed (re) or in the supercoiled (sc) state ($\sigma = -0.06$ see above) was modified either with the OsO_4-pyridine reagent (20 mM OsO_4, 20% pyridine) (lanes 1,2,5 and 6) for 15 min at room temperature or with DEPC for 30 min at room temperature (lanes 3,4, 7 and 8). The strand with the $d(A)_{15}$ tract (lanes 1–4) was labeled after digestion with *Hin*d III-*Sst* and the complementary strand with the $d(T)_{15}$ segment (lanes 5–8) after digestion with *Eco*R I-*Sph* I. **(B)** Sequencing of OsO_4-pyridine and DEPC modified pPS-PP1. The supercoiled (sc) plasmid (lanes 2 and 4) or relaxed (re) plasmid molecules (lanes 1 and 3) were treated with Os,py or DEPC and digested with *Hin*d III-*Sst* I before labelling. Lanes 5 and 6 contained the same material as in lanes 1 and 2 but were electrophoresed for a longer period of time in order to better resolve intensities within the second (closer to the 5′ end) ps dA·dT block. The dC closest to the 5′–5′ bond and a dG residue 16 bases away were also reactive with Os,py (lanes 5 and 6). This result was not observed with the single insert construct pPS-PX1 and may reflect a perturbation exerted by the two inverted ps inserts on the intervening DNA segment. **(C)** Densitogram of the sequencing gel depicting differences between modification patterns within the dT (obtained with OsO_4) sequence of the supercoiled and relaxed pPS-PX1. **(D)** Modification pattern within the dA tract, obtained with DEPC of the supercoiled and relaxed pPS-PX1.

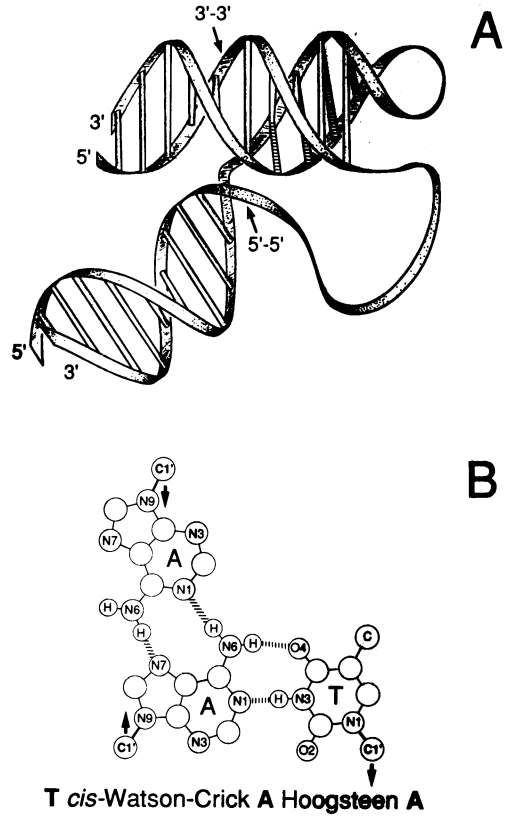

Fig. 6. Schematic model of the triplex structures based upon the observed chemical modification pattern that appears upon negative supercoiling. **(A)** Triplex model. The dA·dT base pairing is of the conventional *cis*-Watson-Crick type (*c-WC*, white bonds). The putative sites of dA·dA Hoogsteen base pairs are drawn with a ladder pattern. The drawing is adapted from Ref. (64). **(B)** Corresponding d(A·A·T) triplets with antiparallel purine strands. The type of dA·dA Hoogsteen base pairing depicted is found in crystals of deoxyadenosine monohydrate (65).

thermodynamic properties of the linear inserts above. The Os,py-sensitivity increases dramatically under topological stress ($-\sigma > -\sigma_{tr}$), with the exception of several bases closest to the 3'-p-3' phosphodiester bond (panel A, lane 6; panel B, lanes 2,6; panel C). More than half of the $d(T)_{15}$ tract is reactive, from which we conclude that the pyrimidine strand is present largely in a single-stranded form except for the 4–5 residues adjacent to the 3'-p-3' junction.

The DEPC modification pattern of the $d(A)_{15}$ sequence of the relaxed molecules reveals an even distribution of intensities (Fig. 5: panel A, lane 3; panel B, lane 3; panel D). The first two residues at the 3' end are less reactive than the others, in accordance with a previous report on the sensitivity of A tracts to DEPC (42). In general, the slightly elevated reactivity of dTs and dAs in the ps inserts of the relaxed plasmids is consistent with the results from previous studies of linear ps-DNA molecules subjected to Os,py and DEPC modification (12). The reaction of the pPS-PX1 and the pPS-PP1 plasmids with DEPC changes dramatically in the supercoiled state. A pronounced modification of the 5–6 centrally located dA residues is superimposed over the uniform pattern of all purine residues. The most modified dA is located precisely in the center of the tract.

DISCUSSION

The structure induced in the ps helix is a novel triple helix

The major results of this study are the demonstration that ps-DNA is a right-handed helix and that negative supercoiling induces a transition to a more relaxed state. The chemical modification patterns in Fig. 5 are similar for both the single pPS-PX1 and the two pPS-PP1 ps inserts and are consistent with the 2-D gel electrophoretic behavior. The differences in reactivity of the purine and pyrimidine strands are compatible neither with a persistent denaturation nor cruciformation as the structural basis of the observed transitions. In particular we note that cruciformation requires the presence of an inverted repeat sequence and results in two extruded hairpins with centrally located loops. Thus, chemical modification occurs at the same locus in both opposing strands. We do not observe such a pattern of reactivity. The pPS-PP1 plasmid contains an 86 bp long inverted repeat sequence (including flanking nucleotides of the vector), which potentially could lead to the hairpin extrusion under topological stress. However, the 2-D gel and chemical modification pattern are very similar to those of pPS-PX1. Cruciformation is known to be sensitive to the base composition of the sequence around and within the loop region (43). The central region of our inverted repeat is dG·dC-rich and therefore has high thermodynamic stability, a circumstance that would favor structural transitions within both of the ps inserts at low superhelix densities.

We propose that another specific conformation arises, namely a triple helix but one distinct in certain respects from that known as H-DNA. The latter forms as the product of an intramolecular rearrangement in negatively supercoiled molecules in which one half of a oligopurine·oligopyrimidine duplex is folded back so that one strand (generally the pyrimidine) is Hoogsteen base paired in the major groove and the second strand looped out (28–31,37–40). The triplex structure also arises with linear DNA and in suitably designed single strand sequences, in which the existence of $d(T\cdot A\cdot T)$ and $d(C^+\cdot G\cdot C)$ triplets has been confirmed by ^{1}H-NMR (44,45).

The DEPC modification pattern (Fig. 5A,B,D) suggests that supercoiling induces a local denaturation of the ps sequence leading to a rearrangement of the purine strand with generation of a central 3–5 bp single-stranded loop. At the same time we deduce from the Os,py-modification pattern that the $d(T)_{15}$ tract is partly but not entirely unstructured. That is, the segment closest to the 3'-p-3' junction shows only weak reactivity, implying that it interacts with the remainder of the dA_{15} tract.

A possible model for a the triple-stranded DNA structure arising from the ps insert is illustrated in Fig. 6. The purine strand folds back from a hairpin loop giving rise to a triple-stranded DNA conformation involving two dA and one dT strands. We estimate that approximately one third of the pyrimidine strand closest to the 3'-p-3' bond interacts with the 5'-half of the purine tract forming *cis*-Watson-Crick hydrogen bonds in an aps helix. The 3'-purine segment completes the triplex via Hoogsteen base pairs and is oriented antiparallel to the other half of the purine strand (Fig. 6B). The rest of the pyrimidine sequence is single-stranded, accounting for its substantially greater sensitivity to Os,py modification. A four-way structure (2 duplexes, one triplex, 1 single-strand) constitutes the base of the triplex, as in the case of H-DNA. The indicated isomer of the $d(A\cdot A\cdot T)$ triplex detected by chemical modification apparently predominates over a second potential configuration in which the pyrimidine segment adjacent to the 5'-p-5' junction pairs with the 3' region of the purine fold-back structure. It is possible that specific 3'-p-3' and 5'-p-5' junctional effects may favor the formation of one isomer over the other.

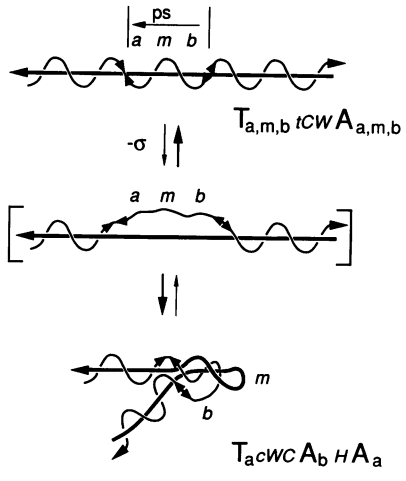

Fig. 7. Suggested mechanism for the observed transition. The arrows point in the 3' direction. The letters *a*, *m* and *b* refer to: (*a*) the 3 to 5 dA/dT residues close to the 3'-3' linkage that are not modified by DEPC or Os,py; (*m*) the DEPC modified 4–5 bases of the A strand (thick line) in the middle of the dA·dT tract; and (*b*) the part close to the 5'–5' linkage where only the T strand (thin line) is sensitive to the chemical reagents. The nomenclature $T_a cWC A_b HA_a$ indicates that part *a* of the T-strand (T_a) is paired with part *b* of the A-strand (A_b) via *cis*-Watson-Crick (*c-WC*) base pairs and that parts *b* and *a* of the A-strand (A_b, A_a) interact by Hoogsteen (*H*) base pairing (cf. Fig. 6B). The steady-state intermediate denatured state is shown in brackets.

Mechanism of the ps-triplex transition

The triplex depicted in Fig. 6 incorporates a new *cis*-Watson-Crick duplex segment constituted by purine and pyrimidine sequences originally located at opposite ends of the insert. The 2-D gels in Fig. 4 reveal a major transition of pPS-EB1 and pPS-PX1 with a midpoint σ_{tr} of ~ -0.036, which we explain by the formation of a triplex structure according to the mechanism depicted in Fig. 7. It is conceptually related to the C-type

cruciform extrusion (46) in the sense that it involves the denaturation of most or all of the insert for initiation of the transition.

Formation of the triplex requires an initial denaturation of the ps insert probably at one of the aps-ps junctions; in its fullest extent the entire insert is involved, followed by winding of the dA strand in the form of a hairpin about the segment of the pyrimidine strand starting at the junction. The transition is driven energetically to completion by formation of the stable aps duplex and by any incremental stabilization afforded by the additional secondary structure of the triplex. The stereochemistry at the base of the triplex probably involves additional unwinding and bending and a corresponding unfavorable transition free energy term, as observed in the B−Z transition (19,24,25), cruciformation (47), and H-DNA formation (48).

Statistical mechanical analysis of the ps-triplex transition

We have undertaken a quantitative assessment of the proposed mechanism and structural assigment by statistical mechanical methods used previously to analyze the B−Z transition, cruciformation and H-DNA formation (19,24,25,48−50). The basis of the analysis is the calculation of the partition function Q describing the distribution of free energy within the population of molecules i as a sum of the statistical weights in the form of the corresponding equilibrium constants k_i (49,50). The latter are generally normalized with respect to a reference state, *e.g.*, the initial structure preceding a transition, so that

$$Q = 1 + \sum_{i>0} w_i k_i$$

degenerate states are assigned an appropriate weighting factor $w_i > 1$.

The probability p_i of a given state k_i equals $w_i k_i / Q$. Thus, the population mean $\langle\xi\rangle$ of a parameter ξ for which each state i has an associated value ξ_i is given by

$$\langle\xi\rangle = \sum_{i\geq 0} \xi_i p_i.$$

In our case, ξ is the mean change in twist accompanying unwinding, i. e., $\langle\Delta Tw\rangle$.

We adopt a zipper model (one nucleation and triplex propagation step per ps insert) in the mechanism of Fig. 7, and consider explicitly the thermodynamics of denaturation as a first step followed by a transition from the denatured state to the triplex structure. This approach is valid even though the denatured species are not populated to a significant extent in the steady state distribution. In generating the configurational partition function Q and the resultant unwinding $\langle\Delta Tw\rangle$, the statistical weights of the microstates are calculated relative to the non-relaxed supercoiled state. Each particular conformation changing the twist of the molecule is stabilized by a corresponding redistribution of the free energy of supercoiling.

$$S = \sum_{m=m_{min}}^{n} \tau(m)\ \sigma_d\ \sigma_j\ s_{ps}^{-m} V_s(\sigma,m,b_o) \cdot \left\{ \sum_{k=k_{min}}^{k_{max}} \sigma_t\ (s_{aps}s_t)^k f(m+1)\ f(m-2k+1) \right\} \quad (3)$$

$$Q = 1 + S|_{\tau(m)\equiv 1} \quad (4)$$

$$\langle\Delta Tw\rangle = Q^{-1}S|_{\tau(m)=-m/h_o+b_o} \quad (5)$$

The contribution to the statistical weight from supercoiling energy (Eq. 2) is given by

$$V_s(\sigma,m,b_o) = \exp\,[-10N\{(\sigma + m/N - b_o h_o/N)^2 - \sigma^2\}] \quad (6)$$

Each term in the first series summation in Eq. 3 represents the initial denaturation of the ps insert (with total length n) by generation of an internal loop. Two nucleation factors (σ_d and σ_j) correspond, respectively, to melting within $d(A)_n \cdot d(T)_n$ inserts in closed circular DNA (51,52) (we assume that the aps and ps duplexes are similar in this respect), and to any enhanced opening at the aps-ap junctions. The equilibrium constant for each stacking interaction in the ps duplexes is s_{ps}. The index m extends from a minimal value m_{min} to the full length of the insert. The factor V_s represents the favorable topological driving force for denaturation and increases with m. Nucleation also involves a loop-weighting function $f(x)$ accounting for the entropic cost of generating a denaturation bubble. We use $f(x) = (x/2 - 2)^{-1.7}$ where x is the number of bases (covalently linked or hydrogen bonded) constituting an internal or hairpin loop (51−53). For large values of the argument x, this function approximates the usual equation used for an internal loop arising from denaturation of m consecutive base pairs: $f(m) = (m + 1)^{-\alpha}$ with $\alpha = 1.5-2$ (1.7 in 51,52); note that $x = 2(m + 1)$. For small loops, our $f(x)$ is similar to limiting equations suggested in careful studies of hairpin molecules (53); we define $f(\leq 5) \equiv 1$.

In Eq. 3 the contributions of denatured states not restructured into the triplex are omitted. Simulations with parameter values appropriate for our data (Fig. 4) show that their statistical weights are negligible, thereby justifying their consideration as steady state intermediates in the mechanism of Fig. 7. Thus, the $f(\xi)$ associated with the denaturation step is cancelled in the formulation of the inner summation of Eq. 3, which accounts for the ensuing process of triplex formation. The latter incorporates a nucleation step (σ_t), and propagation over k steps with an equilibrium specified by the product of a helix-duplex (s_{aps}) and a duplex-triplex (s_t) equilibrium constant. The triplex length index k has a maximum value $k_{max} = \text{int}[(m - l_{min})/2]$ where l_{min} is the minimal number of base pairs required for intramolecular loop formation. The function τ in Eqs. 3 is either unity (in order to generate Q, Eq. 4) or represents in Eq. 5 the twist change generated by a particular microstate as the sum of two steps: denaturation of m base pairs, and triplex nucleation given by b_o, the basal length invariant twist contribution from the triplex (in units of helical turns and relative to the initial aps-ps-aps helical conformation as the reference state). The dA strand in the triplex generates a hairpin loop and the dT strand a larger loop originating at the four-way junction; we neglect the effect of winding the purine hairpin about the pyrimidine strand. The composite entropy factor for triplex formation is thus a product of the two $f(x)$ in Eq. 3.

We have simulated the major experimental transition depicted in Fig. 4 using the above formalism and a selection of values for most of the parameters taken from the literature (Fig. 4C). Assuming the validity of our analysis, we derive the following quantitative information. (i) About half of the equilibrium change in twist of ~ -2.5 helical turns is attributable to the combination of denaturation and helical rewinding into the triplex structure. The other half ($-1.1-1.2$) represents junctional unwinding associated with triplex formation (b_o); the corresponding free energy change is $\sim$ 5 kcal/mole (Eq. 1). This value can be compared to the 18 kcal/mole reported for the B-H transition

(48) in which a substantial bending of the molecule is also involved (54). (ii) The product $\sigma_j\sigma_t$ is obtained as a function of s_t. The fit to the cooperative transition using Eq. 4 is better with values of $\sigma_t > 2$, implying that forming the triplet by complexation of the second purine strand with the duplex is favored thermodynamically (an s_t of 2−5 is equivalent to a free energy reduction of 0.4−1 kcal/mole). The curves *a1* and *a2* in Fig. 4C were calculated with $s_t = 5$ and $\sigma_j\sigma_t = 0.16$; a similar fit could be obtained with values of 2 and 15, respectively. If we associate the above estimate of 5 kcal/mole for $b_o = -1.1$ with the factor for nucleation of the triplex σ_t, the latter has the value $\sim 2\times10^{-4}$, from which $\sigma_j \approx 10^2$ (for $s_t = 5$) or 10^4 (for $s_t = 2$). The corresponding estimates of 3−4 kcal/mole for the enhanced nucleation of denaturation within the ps inserts are compatible with the helix-coil transition measurements of the isolated aps-ps-aps duplexes (see above). (iii) The cooperativity of the major transition (Fig. 4C) is such that a fully concerted but necessarily phenomenological model also accounts for the data. That is, we can represent the degree of transition θ by the relation $\theta = K_tV_s/(1 + K_tV_s)$ in which V_s is given by Eq. 6 and K_t is the apparent equilibrium constant for the duplex-triplex transition of a relaxed molecule. Simulations yield $K_t \approx 3\times10^{-7}$ with $m = 15$ and $b_o = -0.85$ in V_s (Eq. 6); the value for the transition free energy ($-RT\ln K_t$) of 9 kcal/mole is in good agreement with the 10 ± 1 kcal/mole estimated from Eq. 1. Examination of the individual terms generated in Eqs. 4 and 5 indicate that the triplex species with length > 3 (k, Eq. 3) dominate the transition but the latter is not strictly all-or-none. This circumstance would account for the apparent metastability observed in the 2-D gels. That is, once having overcome the nucleation barrier, the population readily achieves an equilibrium distribution, thus migrating as a well defined spot with a mean electrophoretic mobility predicted by Eq. 5. The altered mobility of the remainder of the molecules (in the case of pPS-EB1, Fig. 4A) may reflect a σ-dependent deformation of the ps insert involving another pathway. (iv) The transitions we observe are at lower negative superhelix densities than for all other reactions induced by negative supercoiling and at neutral pH reported to date. The analysis indicates that this feature is due to the lower helical stability of the ps insert compared to any aps sequence and probably some destabilization at the aps-ps junctions. (v) Although we did not model the transition(s) of the pPS-PP1 plasmid, its behavior is compatible with the above results and the stepwise unwinding of dual identical inserts in other circular DNA molecules (24,25).

CONCLUSION

This study establishes that ps-DNA is a right handed helix capable of facile accommodation within a B-DNA segment and also provides evidence for a novel intramolecular triplex based exclusively on the d(A·A·T) triplet. Although the triple-stranded helix constitutes less than half of a helical turn, it is stable at neutral pH and at low ionic strength in the absence of divalent cations. It is worth noting that similar experimental data obtained with the same chemical probes (Os,py and DEPC) constitute the best evidence available to date for the formation of triplex H-DNA within other oligopurine·oligopyrimidine B-DNA sequences (27,37−40). However, H-DNA generally requires for stability the combination of negative supercoiling and acidic pH [in the case of the hemiprotonated d(C^+·G·C) triplet (28,29,31), divalent cations [Mg^{2+} for stabilization of the d(G·G·C) triplet (55)], or long inserts in the case of $d(A)_n\cdot d(T)_n$ sequences [n = 69 (56)]. Only d(T·A·T) triplets have been described to date in relation to H-DNA, although it has been proposed that inserts of $d(G\text{-}A)_{22}\cdot d(T\text{-}C)_{22}$ in negatively supercoiled plasmids adopt a triplex structure designated as *H-DNA with d(A·A·T) triplets in the presence of Zn^{2+} at neutral pH (57,58). In addition, stable triple-stranded r(A·A·U) and rA·d(A·T) have been reported (59,60). Thus, the stabilization of secondary structure by the d(A·A·T), instead of the d(T·A·T) triplet generally observed with H-DNA, may reflect the particular stereochemistry imposed by the rearrangement of the aps-ps-aps insert (Figs. 6 and 7). Our model of the d(A·A·T) triplet (Fig. 6B) places the two purine strands in an antiparallel orientation. This structure is consistent with that proposed in studies of mixed A·T, G·C sequences: triplexes formed from oligonucleotides (61), and triplexes formed from combinations of oligonucleotides and duplexes (62,63).

Our chemical modification experiments were conducted with molecules at negative superhelix densities above the transition midpoint and necessarily reflect the properties of the final structure that arises. It will clearly be of interest to examine the properties of longer sequences, for example to determine $h_{o,ps}$ with greater precision. One can devise other constructs for exploring the properties of ps-DNA under topological stress, some of which would preserve the normal chemical features of B-DNA and thus apply to natural sequences (2). Such molecules will facilitate the search for specific binding proteins and distinct biological roles of ps-DNA.

ACKNOWLEDGEMENTS

We are indebted to D.Hallmann and F.Benseler for their help in synthesis of the 5′-β-cyanoethyl-3′-dimetoxytrityl thymidine phosphoramidite, to G. Heim for technical assistance, and to numerous colleagues for citical reading of the manuscript.

REFERENCES

1. Jovin, T.M., Rippe, K., Ramsing, N.B., Klement, R., Elhorst, W. and Voijtišková, M. (1990) In Sarma, R.H. and Sarma, M.H. (eds.), *Structure and Methods, Volume 3: DNA and RNA*. Adenine Press, Schenectady, New York, pp.155−174.
2. Jovin, T.M. In Eckstein, F. and Lilley, D.M.J. (eds.), *Nucleic Acids and Molecular Biology*, Vol. 5. Springer-Verlag, Berlin/Heidelberg, in press.
3. Pattabiraman, N. (1986) *Biopolymers* **25**, 1603−1606.
4. van de Sande, J.H., Ramsing, N.B., German, M.W., Elhorst, W., Kalish, B.W., Kitzing, E., Pon, R.T., Clegg, R.M. and Jovin, T.M. (1988) *Science* **241**, 551−557.
5. Ramsing, N.B. and Jovin, T.M. (1988) *Nucleic Acids Res.* **16**, 6659−6676.
6. Germann, M.W., Kalish, B.W. and van de Sande, J.M. (1988) *Biochemistry* **27**, 8302−8306.
7. Rippe, K., Ramsing, N.B. and Jovin, T.M. (1989) *Biochemistry* **28**, 9536−9541.
8. Rippe, K., Ramsing, N.B., Klement, R. and Jovin, T.M. (1990) *J. Biomol. Struct. Dynam.* **7**, 1199−1209.
9. Otto, C., Thomas, G.A., Rippe, K., Jovin, T.M. and Peticolas, W.L. (1991) *Biochemistry* **30**, 3062−3069.
10. Germann, M.W., Vogel, H.J., Pon, R.T. and van de Sande, J.M. (1989) *Biochemistry* **28**, 6220−6228.
11. Rippe, K. and Jovin, T.M. (1989) *Biochemistry* **28**, 9542−9549.
12. Klysik, J., Rippe, K. and Jovin, T.M. (1990) *Biochemistry* **29**, 9831−9839.
13. Rippe, K. and Jovin, T.M. *Meth. Enzymol.*, in press.
14. Maxam, A.M. and Gilbert, T. (1980) *Meth. Enzymol.* **65**, 499−560.
15. Klysik, J., Zacharias, W., Galazka, G., Kwinkowski, M., Uszanski, B. and Okruszek, A. (1988) *Nucleic Acids Res.* **16**, 6915−6933.
16. Singleton, C.K. and Wells, R.D. (1982) *Anal. Biochem.* **122**, 253−257.

17. Cozzarelli, N.R., Boles, T.C. and White, J.H. (1990) In Cozzarrelli, N.R. and Wang, J.C. (eds.), *DNA Topology and its Biological Effects*. Cold Spring Harbor University Press, Cold Spring Harbor, pp. 139–184.
18. Horowitz, D.S., and Wang, J.C. (1984) *J. Mol. Biol.* **173**, 75–91.
19. Peck, L.J. and Wang, J.C. (1983) *Proc. Natl. Acad. Sci. USA*, **80**, 6206.
20. Frank-Kamenetskii, M.D. (1990) In Cozzarrelli, N.R. and Wang, J.C. (eds.), *DNA Topology and its Biological Effects*. Cold Spring Harbor University Press, Cold Spring Harbor, pp. 185–215.
21. Benham, C.J. (1990) In Sarma, R.H. and Sarma, M.H. (Eds.), *Structure and Methods, Volume 3: DNA and RNA*. Adenine Press, Schenectady, New York, pp. 255–266.
22. Paleček, E. *CRC Rev. Biochem. Mol. Biol.*, **26**, 151–226.
23. Yagil, G. *CRC Rev. Biochem. Mol. Biol.*, **26**, 475–559.
24. Kelleher, R.J., III, Ellison, M.J., Ho, P.S. and Rich, A. (1986) *Proc. Natl. Acad. Sci. USA* **83**, 6342–6346.
25. Mirkin, S.M., Lyamichev, V.I., Kumarev, V.P., Kobzev, V.F., Nosikov, V.V. and Vologodskii, A.V. (1987) *J. Biomol. Struc. Dyn.* **5**, 79–88.
26. Lyamichev, V.I., Panyutin, I.G. and Frank-Kamenetskii, M.D. (1983) *FEBS Lett.* **153**, 298–302.
27. Courey, A.J. and Wang, J.C. (1983) *Cell* **33**, 817–829.
28. Lyamichev, V.I., Mirkin, S.M. and Frank-Kamenetskii, M.D. (1986) *J. Biomol. Struc. Dyn.* **3**, 667–669.
29. Lyamichev, V.I., Mirkin, S.M. and Frank-Kamenetskii, M.D. (1987) *J. Biomol. Struc. Dyn.* 5, 275–282.
30. Htun, H. and Dahlberg, J.E. (1988) *Science* **241**, 1791–1796.
31. Shimizu, M., Hanvey, J.C. and Wells, R.D. (1989) *J. Biol. Chem.* **264**, 5944–5949.
32. Paleček, E., Boubliková, P., Jelen, F., Krejcová, A., Makaturová, E., Nejedly, K., Pecinka, P. and Vojtíšková, M. (1990) In Sarma, R.H. and Sarma, M.H. (eds.), *Structure & Methods, Volume 3: DNA and RNA*. Adenine Press, Schenectady, NY, pp. 237–253.
33. Galazka, E. Paleček, Wells, R.D. and Klysik, J. (1986) *J. Biol. Chem.* **261**, 7093–7098.
34. Herr, W. (1985) *Proc. Natl. Acad. Sci. USA* **82**, 8009–8013.
35. Johnston, B.H. and Rich, A. (1985) *Cell* **42**, 713–724.
36. Lilley, D.M.J. and Paleček, E. (1984) *EMBO J.* **3**, 1187–1192.
37. Hanvey, J.C., Klysik, J. and Wells, R.D. (1988) *J. Biol. Chem.* **263**, 7386–7396.
38. Vojtíšková, M., Mirkin, S., Lyamichev,V., Voloshin, O., Frank-Kamenetskii, M. and Paleček, E. (1988) *FEBS Lett.* **234**, 295–299.
39. Johnston, B.H. (1988) *Science* **241**, 1800–1804.
40. Voloshin, O.N., Mirkin, S.M., Lyamichev, V.I., Belotserkovskii, B.P. and Frank-Kamenetskii, M.D. (1988) *Nature* **333**, 475–476.
41. Furlong, J.C. and Lilley, D.M.J. (1986) *Nucleic Acids Res.* **14**, 3995–4007.
42. McCarthy, J.G., Williams, L.D. and Rich, A. (1990) *Biochemistry* **29**, 6071–6081.
43. Zheng, G. and Sinden, R.R. (1988) *J. Biol. Chem.* **263**, 5356–5361.
44. Sklenár, V. and Feigon, J. (1990) *Nature* **345**, 836–838.
45. Unemoto, K., Sarma, M.H., Gupta, G., Luo, J. and Sarma, R.H. (1990) *J. Am. Chem. Soc.* **112**, 4539–4545.
46. Lilley, D.M.J., Sullivan, K.M. and Murchie, A.I.H. (1987) In Eckstein, F. and Lilley, D.M.J. (eds.), *Nucleic Acids and Molecular Biology, Vol. 1*. Springer-Verlag, Berlin/Heidelberg, pp. 126–138.
47. Lilley, D.M.J. and Hallam, L.R. (1984) *J. Mol. Biol.* **189**, 179–200.
48. Lyamichev, V.I., Mirkin, S.M., Kumarev, V.P., Baranova, L.V., Vologodskii, A.V. and Frank-Kamenetskii, M.D. (1989) *Nucleic Acids Res.* **17**, 9417–9423.
49. Anshelevich, A.A., Vologodski, A.V. and Frank-Kamenetskii, M.D. (1988) *J. Biomol. Struct. Dyn.* **6**, 247–259.
50. Soumpasis, D.M. and Jovin, T.M. (1987) In Eckstein, F. and Lilley, D.M.J. (eds), *Nucleic Acids and Molecular Biology, Vol. 1*. Springer-Verlag, Berlin/Heidelberg, pp. 85–111.
51. Blake, R.D. and Delcourt, S.G. (1987) *Biopolymers* **26**, 2009–2026.
52. Blake, R.D. and Delcourt, S.G. (1990) *Biopolymers* **29**, 393–405.
53. Scheffler, I.E., Elson, E.L. and Baldwin, R.L. (1970) *J. Mol. Biol.* **48**, 145–171.
54. Stokrová, J., Vojtíšková, M. and Paleček, E. (1989) *J. Biomol. Struc. Dyn.* **6**, 891–898.
55. Kohwi, Y. and Kohwi-Shigematsu, T. (1988) *Proc. Natl. Acad. Sci. USA* **85**, 3781–3785.
56. Fox, K.R. (1990) *Nucleic Acids Res.* **18**, 5387–5391.
57. Bernués, J., Beltrán, R., Casasnovas, J.M. and Azorin, F. (1989) *EMBO J.* **8**, 2087–2094.
58. Bernués, J., Beltrán, R., Casasnovas, J.M. and Azorin, F. (1990) *Nucleic Acids Res.* **18**, 4067–4073.
59. Broitman, S.L., Im, D.D. and Fresco, J.R. (1987) *Proc. Natl. Acad. Sci. USA* 84, 5120–5124.
60. Letai, A.G., Palladino, M.A., Fromm, E., Rizzo, V. and Fresco, J.R. (1988) *Biochemistry* **27**, 9108–9112.
61. Pilch, D.S., Levenson, C. and Shafer, R.H. (1991) *Biochemistry* **30**, 6081–6087.
62. Beal, P.A. and Dervan, P.B. (1991) *Science* **251**, 1360–1363.
63. Lyamichev, V. I., Voloshin, O.N., Frank-Kamenetskii, D. and Soyfer, V.N. (1991) *Nucleic Acids Res.* **19**, 1633–1638.
64. Murchie, A.I.H., Clegg, R.M., v. Kitzing, E., Duckett, D.R., Diekmann, S. and Lilley, D.M.J. (1989) *Nature* **341**, 763–766.
65. Watson, D.G., Sutor, D.J. and Tollin, P. (1965) *Acta. Cryst.* **19**, 111–124.